Med Oncol (2010) 27:134–144
DOI 10.1007/s12032-009-9184-1

ORIGINAL PAPER

Proteomic analysis of the stroma-related proteins in nasopharyngeal carcinoma and normal nasopharyngeal epithelial tissues

Mei-xiang Li · Zhi-qiang Xiao · Yong-heng Chen · Fang Peng · Cui Li · Peng-fei Zhang · Mao-yu Li · Feng Li · Chao-jun Duan · Dan-Juan Li · Hui-xin Yao · Zhu-chu Chen

Received: 7 December 2008 / Accepted: 9 February 2009 / Published online: 26 February 2009

Abstract The stroma surrounding cancer cell population is increasingly recognized as playing an important role in cancer proliferation, invasion, and metastasis. To identify the stromal proteins involved in nasopharyngeal carcinoma (NPC) carcinogenesis, differences in protein expression of the stroma from NPC and normal nasopharyngeal epithelium tissues (NNET) were assessed using a comparative proteomic approach combined with laser capture microdissection (LCM). LCM was performed to purify stromal cells from NPC and NNET, respectively. Proteins between the pooled microdissected tumor and normal stroma were separated by two-dimensional electrophoresis (2-DE) and differential proteins were identified by mass spectrometry (MS). Sixty differential proteins between normal stroma (NS) and tumor stroma (TS) were identified, and the expression of CapG protein was further confirmed by western blotting and immunohistochemical analysis. Our results will be helpful to study the role of stroma in the NPC carcinogenesis and may provide helpful clues for pathogenesis, early diagnosis, and progression of NPC.

Keywords Nasopharyngeal carcinoma · Stroma · Laser capture microdissection · Two-dimensional gel electrophoresis · Mass spectrometry

M.-x. Li · Z.-q. Xiao · F. Peng · C. Li · P.-f. Zhang · M.-y. Li · C.-j. Duan · D.-J. Li · H.-x. Yao · Z.-c. Chen (✉)
Key Laboratory of Cancer Proteomics of Chinese Ministry of Health, Xiangya Hospital, Central South University, 87# Xiangya Road, 410008 Changsha, Hunan Province, China
e-mail: tcbl@xysm.net

M.-x. Li
e-mail: meixiangle@yahoo.com.cn

M.-x. Li · F. Li · H.-x. Yao · Z.-c. Chen
Cancer Research Institute, Xiangya School of Medicine, Central South University, 410078 Changsha, Hunan Province, China

M.-x. Li
Department of Histology and Embryology, University of South China, 421001 Hengyang, Hunan Province, China

Y.-h. Chen
Molecular and Computational Biology, University of Southern California, Los Angeles, CA, USA

Introduction

More recently, it has become clear that analysis of the tumor stroma is of crucial importance to better understand cancer. Stromal cell–epithelial cell interactions play important roles in tumor development, growth, angiogenesis, and metastasis. It is now recognized that a specific environment is necessary for the development and progression of tumors, and tumorigenesis may be a physiological response to an abnormal stromal environment [1, 2]. In addition, modified stromal cells secrete proteases that facilitate tissue destruction, cancer cell migration, and metastasis [3–6]. So, understand the change of stromal proteins will help to study the role of stroma in the nasopharyngeal carcinoma (NPC) carcinogenesis as well as discover the interaction styles of tumor cells and their surrounding microenvironment.

Nasopharyngeal carcinoma is a high-incidence malignancy in southern China and Southeast Asia [7]. Carcinogenesis of NPC is a complex process involving multiple events and steps. Etiologic studies indicated that Epstein-Barr virus (EBV) infection, dietary exposure to carcinogens, and genetic susceptibility are associated with NPC [8, 9]. Though some molecular pathogenesis studies

on NPC have been undertaken successfully on the gene and transcription levels [10, 11], the carcinogenic mechanism is still unclear. In previous studies on NPC, an intense infiltration of lymphocytes and a complexity of cytokine expression in the tumor biopsy specimens have been noticed [12]. The functional role of these lymphocytes and the mechanism of their recruitment are not fully understood. So NPC formation may have an unusual molecular background. In this regard, using stroma as a sample may be an alterative way to study NPC carcinogenesis. However, there has been no report of proteomic research on the NPC stroma.

Proteomic analysis is currently considered to be a powerful tool for global evaluation of protein expression, and has been widely applied in studies of diseases, especially in fields of cancer research. Using clinical tissue samples may be the most direct and persuasive way to find tumor stroma-related proteins by a proteomic approach. A major obstacle, however, to analyze tissue specimens is tissue heterogeneity. Laser capture microdissection (LCM) has been well established as a tool for purifying stromal cells from tissues, overcoming the problem of tissue heterogeneity and cell contamination.

In this study, microdissected stroma cells from NPC and normal nasopharyngeal epithelium tissues (NNET) are used as study objects. LCM was performed to purify stromal cells from the NPC and NNET, respectively; then, high quality two-dimensional electrophoresis (2-DE) and mass spectrometry (MS) were applied to identify stroma-associated proteins. Sixty differential proteins were identified, and the differential protein CapG was validated by western blotting and immunohistochemistry. The differential expression of CapG was significantly up-regulated in the stroma of NPC compared with NNET. The accumulating evidence indicated that CapG is ubiquitously expressed in normal tissues and particularly abundant in macrophages [13, 14], and involves in cell signaling, receptor-mediated membrane ruffling, phagocytosis, and motility [15, 16]. The dysregulation of CapG has been reported in multiple neoplasms, suggesting that CapG may play important roles in tumor development and progression [17, 18]. However, there has been no report on the association of CapG with NPC, and the biological functions of CapG and its significance in NPC are still unknown. Therefore, we further evaluated the association of CapG expression with clincopathological factors by immunohistochemistry, and determined tumors with CapG up-regulation tends to have a more advanced clinical stage and more poor differentiation (WHO III). The results presented here will no doubt shed light on the study of interaction between NPC cells and their surrounding microenvironment, and will help to study the role of stroma plays in the NPC carcinogenesis.

Materials and methods

Tissue collection

For 2-DE and western blotting, 42 fresh NPC tissues and 42 fresh NNET from healthy individuals were obtained from the First Xiangya Hospital of Central South University, China at the time of diagnosis before any therapy with an informed consent. All samples were verified by histopathology before LCM. Among of these tissues, 30 cases were used for 2-DE and 12 cases for western blotting, respectively. Another group of formalin-fixed and paraffin-embedded tissues including 30 cases of NNET and 66 cases of primary NPC (54 males and 12 females, age 27–78 years, average 48 ± 9 years, TNM staging from II to IV) were obtained from the First Xiangya Hospital of Central South University, China, according to institutional regulations, and used for immunohistochemistry. According to the 1978 WHO classification [19], 66 cases of primary NPC were histopathologically diagnosed as differentiated nonkeratinizing squamous-cell carcinoma (WHO type II, moderately differentiated, 12 cases), and undifferentiated carcinoma (WHO type III, poorly differentiated, 54 cases).

LCM

Laser capture microdissection was performed with a Leica AS LMD system (Leica) as described previously [20]. Frozen sections (8 μm) from each NPC and NNET were prepared using a Leica CM 1900 cryostat (Leica) at −25°C. The sections were placed on a membrane-coated glass slides (Leica), fixed in 75% alcohol for 30 s, and stained with 0.5% violet-free methyl green (Sigma). The stained sections were air-dried and then subjected to LCM. Approximately 200,000–250,000 microdissected cells were required for each 2-DE, and 20,000–25,000 microdissected cells were required for each western blotting. Each cell population was determined to be 95% homogeneous by microscopic visualization of the captured cells (Fig. 1). As biopsy tissue specimens from one patient were too small to microdissect enough stromal cells for one time 2-DE, pooled microdissected stromal cells from 10 NPC or NNET were used for each 2-DE.

Two-dimensional electrophoresis (2-DE)

The microdissected tissues were dissolved in lysis buffer (7 M urea, 2 M thiourea, 100 mM DTT, 4% CHAPS, 40 mM Tris, 2% Pharmalyte, 1 mg/ml DNase I) on ice for 1 h with sonicated intermittently, and then centrifuged at 12,000 rpm for 30 min at 4°C. The supernatant was transferred and the concentration of the total proteins was determined using 2-D Quantification kit (Amersham

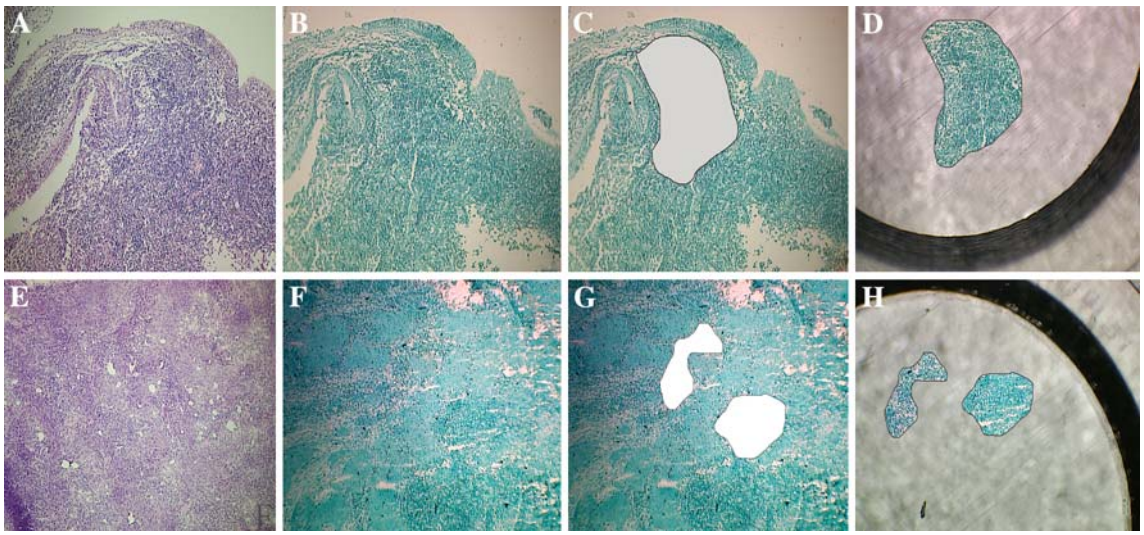

Fig. 1 LCM of NNET and NPC tissues. NNET tissue stained with H&E (**a**), violet-free methyl green before LCM (**b**), after LCM (**c**), and captured normal stroma (**d**); NPC tissue stained with H&E (**e**), violet-free methyl green before LCM (**f**), after LCM (**g**), and captured tumor stroma (**h**)

Biosciences). Next, isoelectric focusing was carried out on an IPGphor system (Amersham Biosciences) using IPG strips (Ph 3-10, 240 mm × 3 mm × 0.5 mm). Second-dimension sodium dodecyl sulfate-polyacrylamide gel electrophoresis (SDS-PAGE) was then performed on an Ettan DALT II system (Amersham Biosciences), which was followed by Blue Silver staining to visualize the protein spots in the 2-DE gels [21].

Image analysis

Two-dimensional electrophoresis maps were obtained by scanning the gels using the Imagescanner (Amersham Biosciences), and analyzed by using a PDQuest system (Bio-Rad Laboratories) according to the manufacturer's protocols. To minimize the contribution of experimental variations, three separate gels were prepared for each microdissected tissue. The densities of the spots were determined after normalization based on the total spot volumes on the gel. Proteins were classified as being differentially expressed between the two types of tissues when spot intensity showed a difference of ≥2-fold variation in tumor stroma in comparison with normal stroma. Protein spots that showed significant changes in densities (paired *t*-test, $P < 0.05$) in a consistent direction (increase or decrease) were considered to be different and selected for further identification.

Protein identification

All the differential protein spots were excised from stained gels using punch, and in-gel trypsin digestion was done as previously described by us [22]. The tryptic peptide was mixed with a α-cyano-4-hydroxycinnamic acid (CCA) matrix solution. One microliter of the mixture was analyzed with a Voyager System DE-STR 4307 MALDI-TOF MS (ABI, Foster City, CA, USA) to get a peptide mass fingerprint (PMF). In PMF map database searching, Mascot Distiller was used to obtain the monoisotopic peak list from the raw MS files. Peptide matching and protein searches against the NCBInr database were performed using the Mascot search engine (http://www.matrixscience.com/) with a mass tolerance of ±50 ppm. The protein spots not identified or identified to be mixture by MALDI-TOF were subjected to analysis of nanoESI-MS/MS (Waters, Manchester, UK). Briefly, the samples were loaded onto a precolumn (320 μm × 50 mm, 5 μm C18 silica beads; Waters) at 30 μl/min flow rates for concentrations and fast desalting through a Waters CapLC autosampler, and then eluted to the reversed-phase column (75 μm × 150 mm, 5 μm, 100 Å; LC Packing) at a flow rate of 200 nl/min after flow splitting for separation. MS/MS spectra were done in data-dependent mode in which up to four precursor ions above an intensity threshold of 7 counts/s were selected for MS/MS analysis from each survey "scan". In tandem MS data database query, the peptide sequence tag (PKL) format file that was generated from MS/MS was imported into the Mascot search engine with a MS/MS tolerance of ± 0.3 Da to search the NCBInr database.

Western blot

Proteins from 12 pairs of microdissected stroma of fresh NPC and NNET were used for western blotting as

previously described by us [22]. Protein concentrations were determined by the Bradford assay using BSA as standard (Protein Assay Kit, Bio-Rad). Briefly, 40 μg of purified protein from each microdissected stroma were separated by 10% SDS-PAGE, and transferred to PVDF membrane (Bio-Rad). The amount of CapG was then detected using anti-CapG (dilution 1:800, Santa Cruze Biotechnology). The results were then visualized using the ECL detection system. All western blot analyses were performed at least three times. The mouse anti-β-actin (dilution 1:5000, Sigma) was detected simultaneously as a loading control.

Immunohistochemistry

Immunohistochemistry was done on paraffin-embedded specimens with anti-CapG (dilution 1:400) using the standard immunohistochemical technique. Immunoreactivity was visualized using 3′, 3′-diaminobenzidine tetrachloride [14] (Sigma-Aldrich), and counterstained with hematoxylin. In negative controls, primary antibodies were replaced by PBS. Immunostaining was blindly evaluated by two independent experienced pathologists in an effort to provide a consensus on staining patterns. For CapG, the numbers of positive cells per core were counted at a magnification of 40×.

Statistical analysis

Statistical analysis was done using SPSS software (version 13.0). To evaluate the extent of CapG expression in NPC and NNET stroma, the number of positively stained cells in each specimen core was determined and the mean number of positive cells per duplicate patient core calculated. For the purpose of analysis, samples were categorized into two groups: those with CapG-positive cell counts > median (high CapG) and those with CapG-positive cell counts ≤ median (low CapG). Significant differences between the expression of CapG and clinicopathologic factors, including age, gender, histologic type/grade (WHO), primary tumor (T) stage, and regional lymph node (N) metastasis were compared by the Mann–Whitney test or Kruskal–Wallis H test. Results were considered to be significant for P-values < 0.05.

Results

Detection of differential proteins of the stroma from NPC and NNET by 2-DE

Proteins from three sets of pooled microdissected stroma of NPC and NNET were analyzed by 2-DE, respectively, and

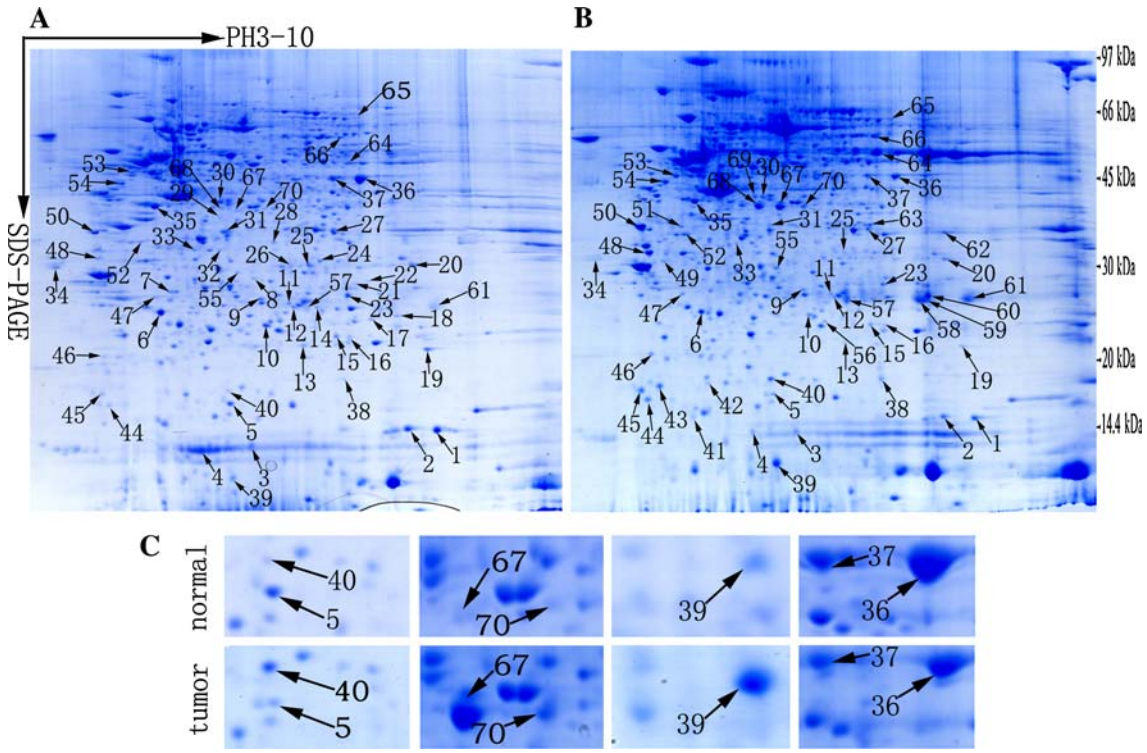

Fig. 2 Representative 2-DE maps of microdissected stroma from NNET (**a**) and NPC (**b**). Seventy differential protein spots identified by MS were marked with arrows. **c** A close-up of the region of the gels showing partial differentially expressed proteins between the stroma of NNET and NPC

Table 1 Differential proteins between the stroma of NPC and NNET identified by MS

No	Proteins	Accession No.	Mr (Da)	PI	Mascot score	Method of identification	Coverage (%)	Fold change[a]
1	Cyclophilin A complexed with dipeptide gly–pro	gil1633054	17,870	7.82	176	MALDI-TOF	58	↓2.44
2	Cyclophilin A complexed with dipeptide gly–pro	gil1633054	17,870	7.82	180	MALDI-TOF	58	↓2.38
3	Ubiquitin-conjugating enzyme E2 N	gil4507793	17,211	6.13	119	MALDI-TOF	68	↓3.85
4	Chain A, transthyretin	gil443295	13,810	5.33	227	ESI-Q-TOF MS	65	↓5.26
5	Superoxide dismutase	gil31615344	16,023	5.7	98	MALDI-TOF	68	↓3.57
6	Rho GDP dissociation inhibitor beta (RhoGDI-β)	gil56676393	23,031	5.1	118	MALDI-TOF	77	↓2.08
7	Gamma-actin	gil178045	26,147	5.65	202	ESI-Q-TOF MS	38	*
	Endothelial cell growth factor 1(platelet-derived)	gil4503445	50,323	5.36	165	ESI-Q-TOF MS	38	*
	Proteasome alpha 3 subunit isoform 1	gil4506183	28,643	5.19	139	ESI-Q-TOF MS	13	*
8	Haloacid dehalogenase-like hydrolase domain	gil14149777	28,746	5.84	102	MALDI-TOF	54	*
9	Enoyl-CoA hydratase, mitochondrial precursor	gil12707570	31,807	8.34	136	ESI-Q-TOF MS	28	↓2.32
10	Peroxiredoxin 3 isoform A precursor	gil5802974	28,017	7.67	187	ESI-Q-TOF MS	33	↓3.85
11	Proteasome beta 10 subunit proprotein	gil4506191	29,203	7.7	171	ESI-Q-TOF MS	25	↓100
12	Protein C14orf166 (CLE)	gil55613379	28,066	6.0	65	MALDI-TOF	24	↓4.17
13	Chain A, Cdc42 complexed with the gtpase binding domain of P21 activated kinase	gil7767047	20,668	5.48	79	MALDI-TOF	33	↓5.88
14	Chain A, triosephosphate isomerase	gil999892	26,807	6.51	81	MALDI-TOF	38	*
15	Proteasome beta 2 subunit	gil4506195	22,993	6.51	148	MALDI-TOF	65	↓2.86
16	Peroxiredoxin	gil4505591	22,324	8.27	80	MALDI-TOF	43	↓2.08
17	Es1 protein isoform IA Precursor	gil134142815	28,495	8.5	104	MALDI-TOF	56	*
18	Hydroxysteroid (17-beta) dehydrogenase 10	gil4758504	26,906	7.66	143	MALDI-TOF	56	*
19	Neuropolypeptide h3	gil913159	21,027	7.42	208	MALDI-TOF	90	↓3.70
20	Guanine nucleotide binding protein, beta-2-like	gil5174447	35,055	7.6	146	MALDI-TOF	64	↓2.22
21	Proline synthetase co-transcribed homolog	gil6005842	30,610	7.09	172	ESI-Q-TOF MS	11	*
22	Methylthioadenosine phosphorylase	gil847724	31,743	6.75	136	ESI-Q-TOF MS	26	*
23	Chain A, triosephosphate isomerase	gil999892	26,807	6.51	108	MALDI-TOF	47	↓2.5
24	Esterase D/formylglutathione hydrolase	gil55957281	28,607	6.92	121	MALDI-TOF	74	*
25	Chain A, human beta-tryptase	gil4699695	27,800	0.46	161	MALDI-TOF	70	↓7.14
26	Chain A, human beta-tryptase	gil4699695	27,800	0.46	110	MALDI-TOF	35	*
27	PDZ and LIM domain 1	gil13994151	36,513	6.56	218	ESI-Q-TOF MS	37	↓2.38
28	26S proteasome-associated pad1 homolog	gil5031981	34,555	6.06	203	ESI-Q-TOF MS	32	*
29	Prohibitin	gil4505773	29,843	5.75	316	ESI-Q-TOF MS	48	*
	Isocitrate dehydrogenase 3 (NAD+) alpha precursor	5031777	40,022	6.47	161	ESI-Q-TOF MS	19	*
30	Serine (or cysteine) proteinase inhibitor, clade B	gil4758906	43,004	5.61	138	MALDI-TOF	44	↓3.57
31	Ribosomal protein P0	gil4506667	34,426	5.71	321	ESI-Q-TOF MS	43	↓9.09
32	Aryl sulfotransferase	gil4096652	34,311	5.81	76	MALDI-TOF	59	*
33	Cytosolic inorganic pyrophosphatase	gil4583153	32,285	5.42	134	ESI-Q-TOF MS	21	↓2.22
34	Fibrinogen beta chain precursor	gil223002	51,358	7.95	135	MALDI-TOF	40	↓100
35	Keratin, type I Cytoskeletal 19 (CK-19)	gil90111766	44,065	5.04	595	ESI-Q-TOF MS	36	↓2.5
	Keratin 19	gil24234699	44,079	5.04	411	ESI-Q-TOF MS	36	↓2.5
36	Enolase 1	gil4503571	47,481	7.01	170	MALDI-TOF	51	↓4.8
37	Enolase 1	gil4503571	47,481	7.01	144	MALDI-TOF	51	↓5.2
38	Smooth muscle protein	gil177175	22,518	8.56	195	ESI-Q-TOF MS	42	↑3.76
39	Chain A, crystal structure of the Mrp14 complexed with chaps	gil20150229	13,159	5.71	106	ESI-Q-TOF MS	76	↑4.29
40	Uncharacterized protein C14orf135 precursor	gil116243177	62,642	5.11	67	MALDI-TOF	27	↑6.16

Table 1 continued

No	Proteins	Accession No.	Mr (Da)	PI	Mascot score	Method of identification	Coverage (%)	Fold change[a]
41	Actin alpha 1 skeletal muscle protein	gil119612724	28,361	5.71	81	MALDI-TOF	18	▲
42	Hypothetical protein LOC51237	gil117938314	21,023	5.37	196	ESI-Q-TOF MS	34	▲
43	Myosin regulatory light chain 9 isoform	gil29568111	19,871	4.8	292	ESI-Q-TOF MS	50	▲
	Regulatory myosin light chain long version	gil33338062	19,937	4.8	205	ESI-Q-TOF MS	50	▲
44	Myosin regulatory light chain MRCL3	gil5453740	19,839	4.67	128	MALDI-TOF	56	↑9.83
45	Myosin regulatory light chain MRCL3	gil5453740	19,839	4.67	74	MALDI-TOF	46	↑3.18
46	Proteasome beta 9 subunit isoform 2 proprotein	gil23110932	22,428	4.92	107	MALDI-TOF	77	↑2.29
47	Laminin-binding protein	gil34234	31,888	4.84	144	MALDI-TOF	43	↑3.18
48	Tropomyosin 1 alpha chain isoform 3	gil63252896	32,774	4.71	318	ESI-Q-TOF MS	20	↑8.07
49	Actin, cytoplasmic 1	gil15277503	40,536	5.55	102	MALDI-TOF	33	▲
50	Tropomyosin 2 (beta) isoform	gil 47519616	23,3028	4.63	278	ESI-Q-TOF MS	29	↑2.53
51	Keratin-31	gil14917115	47,202	4.84	137	ESI-Q-TOF MS	13	▲
52	Vimentin	gil62414289	53,676	5.06	149	MALDI-TOF	38	↑7.52
53	Vimentin	gil62414289	53,676	5.06	129	MALDI-TOF	38	↑2.3
54	Vimentin	gil62414289	53,676	5.06	154	MALDI-TOF	38	↑2.3
55	Fibrinogen gamma chain, isoform CRA_o	gil119625326	47,971	5.45	98	MALDI-TOF	29	↑2.15
56	PYCARD protein	gil48257192	21,326	5.67	107	MALDI-TOF	43	▲
57	Immunoglobulin light chain	gil149673887	23,665	6.97	392	ESI-Q-TOF MS	55	↑5.02
	Chain A, crystal structure of the Fab fragment of a human monoclonal igm cold agglutinin	gil10835792	23,552	5.75	372	ESI-Q-TOF MS	55	↑5.02
	Immunoglobulin light chain	gil149673889	23,705	6.97	321	ESI-Q-TOF MS	55	↑5.02
	Immunoglobulin kappa light chain VLJ region	gil21669395	30,934	8.37	286	ESI-Q-TOF MS	35	↑5.02
58	Immunoglobulin light chain	gil149673887	23,665	6.97	408	ESI-Q-TOF MS	56	↑7.81
	Chain A, crystal structure of the Fab fragment of a human monoclonal Igm cold agglutinin	gil10835792	23,552	5.75	380	ESI-Q-TOF MS	56	↑7.81
59	Immunoglobulin light chain	gil149673887	23,665	6.97	373	ESI-Q-TOF MS	55	▲
	Chain A, crystal structure of the Fab fragment of a human monoclonal Igm cold agglutinin	gil10835792	23,552	5.75	341	ESI-Q-TOF MS	55	▲
	Protein Rei, Bence-Jones	gil229526	23,779	8.75	326	ESI-Q-TOF MS	38	▲
60	Unnamed protein product	gil29446	15,956	7.12	248	ESI-Q-TOF MS	44	↑40.9
	Ig kappa chain V-III (KAU cold agglutinin)	gil106586	23,037	5.75	231	ESI-Q-TOF MS	40	↑40.9
	Beta globin chain	gil66473265	11,480	5.9	218	ESI-Q-TOF MS	38	↑40.9
61	Chain A, crystal structure of a humanized Fab fragment of anti-tissue-factor antibody in complex with tissue factor	gil51247838	23,724	5.95	124	MALDI-TOF	56	↑15.4
62	Annexin A2 isoform 2	gil4757756	38,808	8.32	183	MALDI-TOF	37	▲
63	Hypothetical protein LOC642889	gil89061136	14,662	8.35	169	MALDI-TOF	56	▲
64	Fibrin beta	gil223002	51,358	7.19	119	MALDI-TOF	33	↑15.4
65	Periostin, osteoblast specific factor	gil55661656	90,714	8.08	92	MALDI-TOF	23	↑3.64
66	Transforming growth factor, beta-induced	gil4507467	75,261	7.62	224	ESI-Q-TOF MS	13	↑2.03
67	Fibrinogen beta chain	gil119625339	40,167	6.95	280	MALDI-TOF	83	↑34.5
68	Chain B, crystal structure of fibrinogen fragment D	gil2781208	38,081	5.84	98	MALDI-TOF	31	↑34.5
69	Serum albumin precursor	gil6650826	30,084	6.97	89	MALDI-TOF	38	▲
70	Gelsolin-like capping protein isoform 9 (CapG)	gil55597035	38,779	5.88	166	MALDI-TOF	32	↑4.22

Mr molecular weight; p*I* isoelectric point

* Expressed only in the stroma of NPC

▲ Expressed only in the stroma of NNET

[a] Fold change: tumor stroma/normal stroma: ↑ up-regulated, ↓ down-regulated

stained with Coomassie blue staining (Fig. 2), the gels were subjected to PDQuest imaging analysis. 2-DE maps of the stroma of NPC and NNET obtained between pH 3 and 10 displayed approximately 1,158 spots each. Seventy protein spots that have consistent differences (≥2-fold, $P < 0.05$) between the tumor and normal stroma in triplicate experiments were chosen as differential protein spots and subjected to MS analysis. These differentially expressed protein spots were illustrated with arrows in Fig. 2a, b. Close-up of the region of the gels showing differentially expressed protein between tumor and normal stroma was shown in Fig. 2c.

Identification of differential expression proteins by MS

All of 70 differential protein spots were excised from the stained gels, and analyzed by MS. A total of 60 differential proteins were identified (Table 1). Twenty-two of these 60 protein spots were up-regulated and 38 were down-regulated in the stroma of NPC compared with NNET. A representative MALDI-TOF MS map and database query result of spot 70 are shown in Fig. 3. A total of 34 monoisotopic peaks were input into Mascot search engine to search the NCBInr database, and the query result showed that protein spot 70 was CapG (Fig. 3a, b). Overall, the differentially expressed proteins in the stroma of NPC and NNET were able to be divided into the following groups based on their functions using information obtained from the Swiss-Prot and NCBInr websites: signal transduction and cell communication (17%), cell growth and/or maintenance (22%), energy metabolism (15%), protein metabolism (25%), transportation (3%), apoptosis (2%), immune response (3%), etc. including approximately 17% of the proteins are of unknown function.

Validation of CapG expression by western blotting

Western blotting was done to confirm differential expression of CapG in the 12 pairs of microdissected stroma of NPC and NNET. Equal protein loading was proved by the parallel western blotting of β-actin. As shown in Fig. 4a, CapG was notably up-regulated in the stroma of NPC compared with NNET ($P = 0.025$).

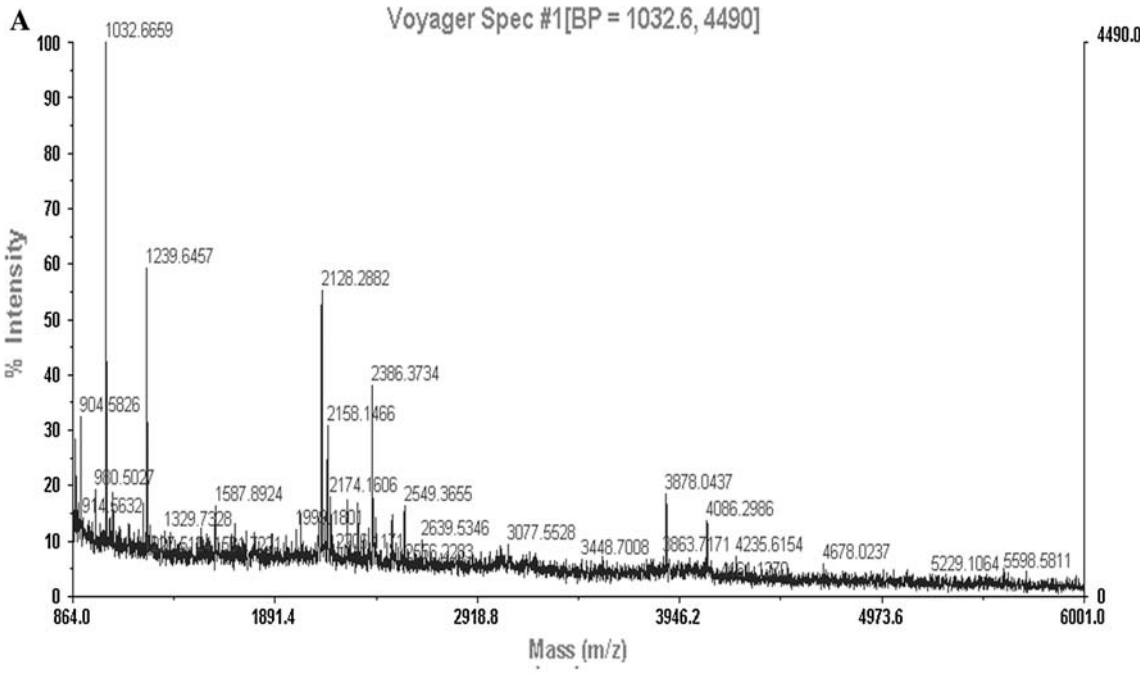

Fig. 3 MALDI-TOF MS analysis of differential protein spot 70. **a** The MALDI-TOF MS mass spectrum of protein spot 70 identified as CapG according to the matched peaks was shown. **b** Protein sequence of CapG was shown, and matched peptides were underlined

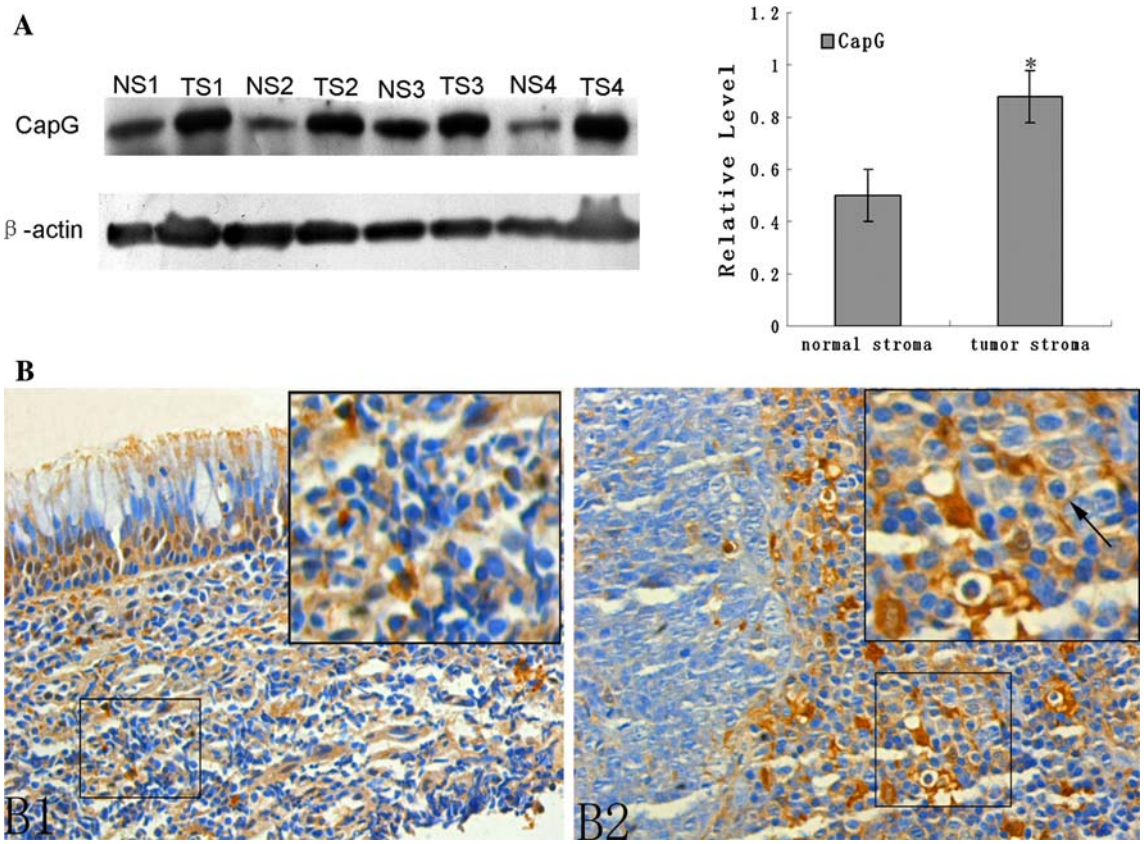

Fig. 4 Validation of differentially expressed proteins. A representative result showing changes in the expression levels of CapG in microdissected stroma from NNET and NPC tissue by western blot analysis (**a**) and immunohistochemistry (**b**). Histogram shows the relative expression levels of CapG in 12 tumor stroma (TS) and 12 normal stroma (NS) as determined by densitometric analysis ($P = 0.025$). Immunohistochemistry of CapG, weak staining in the stroma of NNET (**B1**), strong staining in the stroma of primary NPC (**B2**), it was not detected in cancer cells. Original magnification, ×400

Detection of the expression of CapG in NPC and NNET by immunohistochemistry

The expression of CapG was further detected using immunohistochemistry in 66 cases of primary NPC and 30 cases of NNET. Distinct CapG immunostaining was evident in tumor stroma (Fig. 4b2). However, very weak staining was detectable in those of normal stroma (Fig. 4b1). Additionally, this protein was not detected in cancer cells (Fig. 4b2). However, some nucleuses of epithelial cell were stained (Fig. 4b1). Statistical analysis indicated CapG was significantly up-regulated in the TS versus NS (Table 2, $P < 0.01$). The immunohistochemical result confirmed the differential expression and stromal location of CapG in NPC and NNET. The correlation of several clinicopathologic factors with CapG expression status in 66 cases of primary NPC was shown in Table 2. Tumors with CapG up-regulation tends to have a more advanced clinical stage and more poor differentiation (WHO III) ($P < 0.05$; Table 2). The expression levels of CapG did not correlate with the patients' age, gender, primary tumor stage, and regional lymph node metastasis.

Discussion

Today there is evidence indicating that tumor growth and progression is dependent on the malignant potential of the tumor cells as well as on the multidirectional interactions of local factors produced by the stroma cells [3, 4, 23, 24]. However, the exact mechanisms of tumor–stroma interactions are poorly understood. NPC is one of the most common cancers in Chinese and Asian ancestry [7]. The 5-year survival rate for NPC patients remains 50–60% and the majority of patients are subjected to affliction invasion and metastasis [25, 26]. Our recent studies have identified certain proteins differentially expressed between normal nasopharyngeal epithelial and NPC cells, which might associate with the pathogenesis of NPC [20, 27]. In this study, we screened for differentially expressed proteins in the stroma of NNET and NPC tissue by 2-DE and MS. As a

Table 2 Relationships between CapG expression and clinicopathologic factors in NPC

Variables	CapG			
	n	Low	High	*P*
Group				
NNET	30	22	8	0.000*
NPC	66	12	54	
Age				
≤50	31	10	21	0.340
>50	35	13	22	
Gender				
Male	54	15	39	0.174
Female	12	5	7	
Histology type (WHO)				
WHO II	12	6	6	0.011*
WHO III	54	10	44	
Primary tumor (T) stage				
T1	18	5	13	0.917
T2	23	7	16	
T3	20	7	11	
T4	5	1	4	
Regional lymph node (N) metastasis				
N0	7	2	5	0.926
N1	11	3	8	
N2	31	6	25	
N3	17	4	13	
Clinical stage				
II	7	5	2	0.022*
III	38	8	0	
IV	21	5	16	

* $P < 0.05$ or 0.01 by Mann–Whitney test or Kruskal–Wallis H test

result, 60 differential proteins were successfully identified and they were involved in a variety of biological processes, such as signal transduction and cell communication, energy metabolism, protein metabolism, cell growth and/or maintenance, immune response, transport, and apoptosis (Table 1).

Proteomic analysis is currently considered to be a powerful tool for global evaluation of protein expression, and proteomics has been widely applied in analysis of diseases, especially in fields of cancer research. 2-DE is a classical proteomic technique, which was widely used for proteomic research. Differential protein expression profiling is a crucial part of proteomics, which are able to efficiently provide accurate and reproducible differential expression values for proteins in two or more biological samples. Differential proteome analysis of the stroma of NPC and NNET allows the identification of aberrantly expressed proteins that might provide key information for understanding the carcinogenesis of NPC. However, differential proteomic study of the stroma of NPC has been hampered by NPC cells and nasopharyngeal epithelial cells. LCM has made it possible to isolate pure cell populations from heterogeneous tissue [28], which will provide the possibility and accuracy of screening for proteins associated with stroma by proteomic analysis using tissue samples [29–31].

CapG, a 348-amino acid protein, belongs to the family of actin-binding protein, which is ubiquitously expressed in normal tissues and particularly abundant in macrophages [13, 14], and involves in cell signaling, receptor-mediated membrane ruffling, phagocytosis, and motility [15, 16]. Dysregulation of actin-based motility is a prominent factor in cell transformation and is probably associated with carcinogenesis [17, 18]. The overexpression of CapG in various types of human malignancies has been demonstrated, such as pancreatic cancer cells [32], oral squamous-cell carcinoma [33], etc. Recently study of Cheng et al. [20, 27] discovered that CapG was downregulated in NPC cells compared with normal nasopharyngeal epithelial cells. While, in our study, CapG was upregulated in the stroma cells of NPC compared with normal nasopharyngeal epithelial tissues. Our results of immunohistochemistry confirmed the valid of the two research results. CapG as a tumor promoter, could modulate invasive properties of cells during tumorigenesis [34]. CapG, this protein may act at several levels including cytoskeletal reorganization, gene transcription, and modulation of the signaling pathways. In the present study, CapG was highly expressed in the stroma cells of NPC. Although it is not yet fully elucidated, the role of CapG in cancer-associated stroma is certainly an interesting issue due to the highlighted significance of tumor–stromal interactions by recent researches [35, 36]. Our study indicates that CapG possibly plays a role in the complex interaction between NPC cells and the surrounding host tissue.

The stroma proteins have important functions in the tumor microenvironment involving in a variety of biological processes. For example, we found a significant number of molecules involved in cytoskeletal cell signaling, such as PDZ and LIM domain 1, TGF-β, vimentin, periostin, RhoGDI-β, tropomyosin etc. We also detected the presence of actin-binding protein such as CapG, and that may play a key role in the regulation of cellular motility. This partly explained why proteins involved in cell growth and/or maintenance account for a major percent in the identified stroma proteins. Even though few of these differential stromal proteins were investigated in NPC, the potential value of these proteins involved in the development of NPC deserves further investigation.

In this study, LCM and proteomic approach were used to screen for differential proteins in the stroma of NPC and NNET. Our data have demonstrated the feasibility of using a

proteomic strategy coupled with LCM to identify stromal proteins associated with NPC carcinogenesis. Our study is a first step toward identifying a protein profile of the stoma of NPC and NNET. Although great efforts will be required to elucidate the functions and molecular mechanisms of the stromal proteins in NPC, the identified proteins in this experiment may be used in future studies of carcinogenesis, and will be helpful to study the role of stroma in the NPC carcinogenesis, as well as discover the interaction mode between NPC cells and their surrounding microenvironment.

Acknowledgment This work was supported by a grant from Key research program from the Science and Technology Committee of Hunan Province, China (04XK1001, 06SK2004), National Natural Sciences Foundation of China (30500558, 30670990), Program for New Century Excellent Talents in University (NCET) (2007-70), National Natural Science Foundation of China (30670990, 30871189).

References

1. Bissell MJ, Radisky D. Putting tumours in context. Nat Rev Cancer. 2001;1(1):46–54. doi:10.1038/35094059.
2. Tlsty TD. Cell-adhesion-dependent influences on genomic instability and carcinogenesis. Curr Opin Cell Biol. 1998; 10(5):647–53. doi:10.1016/S0955-0674(98)80041-0.
3. Liotta LA, Kohn EC. The microenvironment of the tumour–host interface. Nature. 2001;411(6835):375–9. doi:10.1038/35077241.
4. Jung YD, Ahmad SA, Liu W, Reinmuth N, Parikh A, Stoeltzing O, et al. The role of the microenvironment and intercellular cross-talk in tumor angiogenesis. Semin Cancer Biol. 2002;12(2):105–12. doi:10.1006/scbi.2001.0418.
5. Quaranta V, Giannelli G. Cancer invasion: watch your neighbourhood!. Tumori. 2003;89(4):343–8.
6. Bogenrieder T, Herlyn M. Axis of evil: molecular mechanisms of cancer metastasis. Oncogene. 2003;22(42):6524–36. doi: 10.1038/sj.onc.1206757.
7. Yu MC, Yuan JM. Epidemiology of nasopharyngeal carcinoma. Semin Cancer Biol. 2002;12(6):421–9. doi:10.1016/S1044579X02000858.
8. Raab-Traub N. Epstein-Barr virus in the pathogenesis of NPC. Semin Cancer Biol. 2002;12(6):431–41. doi:10.1016/S1044579X0200086X.
9. Xiong W, Zeng ZY, Xia JH, Xia K, Shen SR, Li XL, et al. A susceptibility locus at chromosome 3p21 linked to familial nasopharyngeal carcinoma. Cancer Res. 2004;64(6):1972–4. doi: 10.1158/0008-5472.CAN-03-3253.
10. Yau WL, Lung HL, Zabarovsky ER, Lerman MI, Sham JS, Chua DT, et al. Functional studies of the chromosome 3p21.3 candidate tumor suppressor gene BLU/ZMYND10 in nasopharyngeal carcinoma. Int J Cancer. 2006;119(12):2821–6. doi:10.1002/ijc.22232.
11. Hui AB, Or YY, Takano H, Tsang RK, To KF, Guan XY, et al. Array-based comparative genomic hybridization analysis identified cyclin D1 as a target oncogene at 11q13.3 in nasopharyngeal carcinoma. Cancer Res. 2005;65(18):8125–33. doi:10.1158/0008-5472.CAN-05-0648.
12. Buettner M, Meyer B, Schreck S, Niedobitek G. Expression of RANTES and MCP-1 in epithelial cells is regulated via LMP1 and CD40. Int J Cancer. 2007;121(12):2703–10. doi:10.1002/ijc.23018.
13. Yu FX, Johnston PA, Sudhof TC, Yin HL. gCap39, a calcium ion- and polyphosphoinositide-regulated actin capping protein. Science. 1990;250(4986):1413–5. doi:10.1126/science.2255912.
14. Dabiri GA, Young CL, Rosenbloom J, Southwick FS. Molecular cloning of human macrophage capping protein cDNA. A unique member of the gelsolin/villin family expressed primarily in macrophages. J Biol Chem. 1992;267(23):16545–52.
15. Witke W, Li W, Kwiatkowski DJ, Southwick FS. Comparisons of CapG and gelsolin-null macrophages: demonstration of a unique role for CapG in receptor-mediated ruffling, phagocytosis, and vesicle rocketing. J Cell Biol. 2001;154(4):775–84. doi:10.1083/jcb.200101113.
16. Parikh SS, Litherland SA, Clare-Salzler MJ, Li W, Gulig PA, Southwick FS. CapG(−/−) mice have specific host defense defects that render them more susceptible than CapG(+/+) mice to *Listeria monocytogenes* infection but not to *Salmonella enterica* serovar Typhimurium infection. Infect Immun. 2003;71 (11):6582–90. doi:10.1128/IAI.71.11.6582-6590.2003.
17. Kassis J, Lauffenburger DA, Turner T, Wells A. Tumor invasion as dysregulated cell motility. Semin Cancer Biol. 2001;11(2): 105–17. doi:10.1006/scbi.2000.0362.
18. Yamazaki D, Kurisu S, Takenawa T. Regulation of cancer cell motility through actin reorganization. Cancer Sci. 2005; 96(7):379–86. doi:10.1111/j.1349-7006.2005.00062.x.
19. Shanmugaratnam K, Sobin LH. The World Health Organization histological classification of tumours of the upper respiratory tract and ear. A commentary on the second edition. Cancer. 1993; 71(8):2689–97. doi:10.1002/1097-0142(19930415)71:8<2689::AID-CNCR2820710843>3.0.CO;2-H.
20. Cheng AL, Huang WG, Chen ZC, Peng F, Zhang PF, Li MY, et al. Identification of novel nasopharyngeal carcinoma biomarkers by laser capture microdissection and proteomic analysis. Clin Cancer Res. 2008;14(2):435–45. doi:10.1158/1078-0432.CCR-07-1215.
21. Candiano G, Bruschi M, Musante L, Santucci L, Ghiggeri GM, Carnemolla B, et al. Blue silver: a very sensitive colloidal Coomassie G-250 staining for proteome analysis. Electrophoresis. 2004;25(9):1327–33. doi:10.1002/elps.200305844.
22. Yang YX, Xiao ZQ, Chen ZC, Zhang GY, Yi H, Zhang PF, et al. Proteome analysis of multidrug resistance in vincristine-resistant human gastric cancer cell line SGC7901/VCR. Proteomics. 2006;6(6):2009–21. doi:10.1002/pmic.200402031.
23. Tlsty TD, Hein PW. Know thy neighbor: stromal cells can contribute oncogenic signals. Curr Opin Genet Dev. 2001;11(1):54–9. doi:10.1016/S0959-437X(00)00156-8.
24. Park CC, Bissell MJ, Barcellos-Hoff MH. The influence of the microenvironment on the malignant phenotype. Mol Med Today. 2000;6(8):324–9. doi:10.1016/S1357-4310(00)01756-1.
25. Vokes EE, Liebowitz DN, Weichselbaum RR. Nasopharyngeal carcinoma. Lancet. 1997;350(9084):1087–91. doi:10.1016/S0140-6736(97)07269-3.
26. Ahmad A, Stefani S. Distant metastases of nasopharyngeal carcinoma: a study of 256 male patients. J Surg Oncol. 1986; 33(3):194–7. doi:10.1002/jso.2930330310.
27. Cheng AL, Huang WG, Chen ZC, Zhang PF, Li MY, Li F, et al. Identificating cathepsin D as a biomarker for differentiation and prognosis of nasopharyngeal carcinoma by laser capture microdissection and proteomic analysis. J Proteome Res. 2008; 7(6):2415–26. doi:10.1021/pr7008548.
28. Emmert-Buck MR, Bonner RF, Smith PD, Chuaqui RF, Zhuang Z, Goldstein SR, et al. Laser capture microdissection. Science. 1996;274(5289):998–1001. doi:10.1126/science.274.5289.998.
29. Shekouh AR, Thompson CC, Prime W, Campbell F, Hamlett J, Herrington CS, et al. Application of laser capture microdissection combined with two-dimensional electrophoresis for the discovery of differentially regulated proteins in pancreatic ductal

adenocarcinoma. Proteomics. 2003;3(10):1988–2001. doi:10.1002/pmic.200300466.
30. Whiteman HJ, Weeks ME, Dowen SE, Barry S, Timms JF, Lemoine NR, et al. The role of S100P in the invasion of pancreatic cancer cells is mediated through cytoskeletal changes and regulation of cathepsin D. Cancer Res. 2007;67(18):8633–42. doi:10.1158/0008-5472.CAN-07-0545.
31. Hansson O, Strom K, Guner N, Wierup N, Sundler F, Hoglund P, et al. Inflammatory response in white adipose tissue in the non-obese hormone-sensitive lipase null mouse model. J Proteome Res. 2006;5(7):1701–10. doi:10.1021/pr060101h.
32. Thompson CC, Ashcroft FJ, Patel S, Saraga G, Vimalachandran D, Prime W, et al. Pancreatic cancer cells overexpress gelsolin family-capping proteins, which contribute to their cell motility. Gut. 2007;56(1):95–106. doi:10.1136/gut.2005.083691.
33. Nomura H, Uzawa K, Ishigami T, Kouzu Y, Koike H, Ogawara K, et al. Clinical significance of gelsolin-like actin-capping protein expression in oral carcinogenesis an immunohistochemical study of premalignant and malignant lesions of the oral cavity. BMC Cancer. 2008;8:39. doi:10.1186/1471-2407-8-39.
34. De Corte V, Van Impe K, Bruyneel E, Boucherie C, Mareel M, Vandekerckhove J, et al. Increased importin-beta-dependent nuclear import of the actin modulating protein CapG promotes cell invasion. J Cell Sci. 2004;117(Pt 22):5283–92. doi:10.1242/jcs.01410.
35. Kenny PA, Bissell MJ. Tumor reversion: correction of malignant behavior by microenvironmental cues. Int J Cancer. 2003;107(5):688–95. doi:10.1002/ijc.11491.
36. Mueller MM, Fusenig NE. Friends or foes—bipolar effects of the tumour stroma in cancer. Nat Rev Cancer. 2004;4(11):839–49. doi:10.1038/nrc1477.